Nanoscale

PAPER

View Article Online
View Journal | View Issue

Cite this: *Nanoscale*, 2017, **9**, 1599

A silica-based SERS chip for rapid and ultrasensitive detection of fluoride ions triggered by a cyclic boronate ester cleavage reaction†

Jian Zhang,*[a] Lifang He,[a] Peirong Chen,[a] Chao Tian,[a] Jianping Wang,[b] Bianhua Liu,[b] Changlong Jiang*[b] and Zhongping Zhang[b,c]

Received 24th September 2016,
Accepted 18th December 2016

DOI: 10.1039/c6nr07545b

www.rsc.org/nanoscale

Chemical sensing for the convenient detection of trace aqueous fluoride ions (F^-) has been widely explored with the use of various sensing materials and techniques. It still remains a challenge to achieve ultrasensitive but simple, rapid, and inexpensive detection of F^- for environmental monitoring and protection. Here we reported a novel surface-enhanced Raman scattering (SERS) nanosensor, fluorescein phenylboronic acid covalently linked to 1,4-dimercapto-2,3-butanediol modified Au@Ag NPs by a cyclic boronate ester (Flu-PBA-Diol-Au@Ag NPs), for the rapid and ultrasensitive detection of F^-. Once the Flu-PBA approached the surface of Au@Ag NPs, the Raman signals of Flu-PBA were remarkably enhanced due to the strong SERS effect. However, the presence of F^- will induce the cleavage reaction of the cyclic boronate ester into the trifluoroborate anion (3F-Flu-PBA) and diol. The 3F-Flu-PBA molecules exfoliated from the surface of Au@Ag NPs, and the SERS signals of the nanosensor were quenched. Following the sensing mechanism, a silica-based SERS chip has been fabricated by the assembly of Flu-PBA-Diol-Au@Ag NPs on a piece of silicon wafer. The silica-based SERS chips showed high sensitivity for aqueous F^-, and the limit of detection (LOD) could reach as low as 0.1 nM. Each test using the SERS chip only needs a droplet of 20 μL sample and is accomplished within ~10 min. The silica-based SERS chip has also been applied to the quantification of F^- in tap water and lake water.

Introduction

Among all anions, fluoride, having the smallest ionic radius, highest charge density, and a hard Lewis basic nature, has arisen as an attractive target for sensor design owing to its association with a diverse array of biological, medical, and technological processes.[1–3] An appropriate amount of fluoride ingestion is essential to the prevention of dental caries and osteoporosis and promotes healthy bone growth.[4–6] However, excessive fluoride intake would cause serious health problems to human beings, such as metabolism disorders, skeletal disease, mottled teeth, immunological damage and DNA damage.[7,8] In order to prevent such problems, the United States Environmental Protection Agency (EPA) recommends the optimal fluoride level at 0.7–1.2 mg L^{-1} in drinking water.[9] The World Health Organization (WHO) has requested the local government to monitor the fluoride levels in water supplies at any time and stimulated the development of new methods for the quantitative analysis of fluoride.[10] The sensitive fluoride ion assays are usually performed with a wealth of established techniques including ion chromatography, ^{19}F NMR, fluoride ions selective electrodes and fluorescence capillary electrophoresis.[11–14] As these analyses are expensive, time-consuming, and require tedious sample pretreatments and enrichments, there exists a great demand to develop an ultrasensitive, simple, rapid and reliable assay of fluoride ions for improving drinking water safety and environmental protection.

With the advantages of high sensitivity, unique spectroscopic fingerprint and nondestructive data collection, the surface-enhanced Raman scattering (SERS) technique has become one of the most powerful spectroscopic tools for the identification and detection of chemical[15–17] and biological species.[18–20] It has been recognized that the cooperative effects of electromagnetic (EM) and chemical enhancements (CM) result in a remarkable boost of the SERS signal,[21,22]

[a]*Department of Applied Chemistry, Anhui Agricultural of University, Hefei, Anhui 230036, China. E-mail: jianzhang@ahau.edu.cn*
[b]*CAS Center for Excellence in Nanoscience, Institute of Intelligent Machines, Chinese Academy of Sciences, Hefei, Anhui 230031, China. E-mail: cljiang@iim.ac.cn*
[c]*School of Chemistry and Chemical Engineering, Anhui University, Hefei, Anhui 230601, China*

†Electronic supplementary information (ESI) available. See DOI: 10.1039/c6nr07545b

and the EM enhancements are mainly responsible for the occurrence of SERS which leads to a 10^6–10^{15} enhancement factor dependent on the strength of the EM field on the surface of metal nanomaterials.[23,24] Although metal nanomaterial based SERS provides gratifying results for the SERS signal to the target molecules,[25–27] a remarkable enhancement in Raman intensity is usually observed in resonant dyes (such as fluorescein, rhodamine-6G and crystal violet) because of their high Raman scattering cross-sections.[28,29] Most target analytes including drugs, pesticides and inorganic species with small scattering cross-sections are Raman-inactive, and the resulting signals are usually extremely weak even if enhanced. Thus, it is essential to develop the SERS technique for the detection of Raman-inactive molecules with much smaller scattering cross-sections. One of the most prevalent ways is to utilise the molecular interactions of the hydrogen bond, charge-transfer reaction and complexing coordination to amplify the Raman signals of prearranged molecules for the detection of Raman-inactive analytes.[30–32] Disadvantageously, these interaction-based approaches of Raman-inactive analytes are only performed in the solution system, which would be easily affected by similar molecules, media or environments, leading to the unambiguous problem for the determination with false positives from the unavoidable aggregation of metal nanoparticles in the real sample.[33,34] To the best of our knowledge, SERS nanosensors for the detection of Raman-inactive fluoride ions in the real sample have not been previously reported due to its extremely weak Raman signals and the unsolved problem of the solution system in selectivity, sensitivity and reliability.

Herein, we combined the SERS and the specific interaction between the boron atom and the fluoride ion together to develop a highly sensitive and selective chemosensor for the rapid detection of F^- in practical applications. Through the formation of the cyclic boronate ester between phenylboronic acid and diol, the surface of 1,4-dimercapto-2,3-butanediol (Diol) modified silver coated gold nanoparticles (Diol-Au@Ag NPs) can covalently link with the Raman signal molecule fluorescein phenylboronic acid (Flu-PBA), leading to a strong surface-enhanced Raman effect and signal readouts. The presence of F^- will induce the cleavage reaction of the cyclic boronate ester into the trifluoroborate anion (3F-Flu-PBA) and diol. The 3F-Flu-PBA molecules exfoliated from the surface of Diol-Au@Ag NPs, and the SERS signals of the nanosensor were quenched. On the basis of the above experimental results, silica-based SERS chips were prepared *via* the assembly of Flu-PBA-Diol-Au@Ag NPs onto a piece of silicon wafer. The silica-based SERS chip was used as a convenient indicator of the F^- level with the use of only 20 μL samples, and the whole test can be accomplished within ~10 min. Meanwhile, the developed simple and rapid SERS-based chip sensor also exhibits high sensitivity and reliability in the detection of F^- in real samples, and thus opens a novel avenue to fabricate SERS-based sensors for Raman-inactive molecules.

Experimental

Chemicals and materials

Sodium citrate, ammonia solution, hydrogen peroxide (H_2O_2, 30%), sulfuric acid (H_2SO_4, 98%), nitric acid (HNO_3, 65%), silver nitrate ($AgNO_3$, 99%), chloroauric acid ($HAuCl_4{\cdot}4H_2O$, 99.9%), dimethylformamide (DMF), acetone, methanol, chloroform, NaOH, KF, NaCl, KBr, $NaNO_3$, Na_2SO_4, Na_2HPO_4, Na_2CO_3 and $NaHCO_3$ were purchased from the Sinopharm Chemical Reagent Co., Ltd. Fluorescein isothiocyanate isomer I (Fitc, >95%), 1,4-dimercapto-2,3-butanediol (Diol) and 3-aminobenzeneboronic acid were supplied by Aladdin reagent Co., Ltd. 3-Aminopropyltriethoxysilane (3-APTS) was obtained from Sigma-Aldrich. All reagents were used without further purification. Ultrapure water (18.2 MΩ cm) was produced using a Millipore water purification system and used for all solution preparations. Tap water samples were collected from our lab, the lake water sample was obtained from a local lake.

Preparation of 1,4-dimercapto-2,3-butanediol modified Au@Ag nanoparticles (Diol-Au@Ag NPs)

Typically, 0.25 mL of 0.1 M $HAuCl_4$ was added to 100 mL of ultrapure water and then heated to boiling under magnetic stirring. After quickly injecting 1.5 mL of 1% trisodium citrate, the mixed solution was refluxed for ~30 min until it became wine red and 30 nm Au NPs were synthesized. 4 mL of 1% trisodium citrate was rapidly injected into the above boiling solution. Then 17 mL of 1 mM $AgNO_3$ was added dropwise into the above mixture at a rate of one drop per 30 s. Silver nitrate was reduced with trisodium citrate and the resultant silver continuously grew on the surface of the Au seeds. After the wine red solution changed to orange yellow, the solution was stirred for 30 min and the Au@Ag NPs were obtained. Meanwhile, Ag NPs with ~30 nm were prepared by the reduction of $AgNO_3$ with trisodium citrate in water.[33] The Au, Ag and Au@Ag NP concentrations are 0.26, 0.62 and 0.26 nM, respectively, which are calculated using Beer's law and the extinction coefficients. 10.0 μM 1,4-dimercapto-2,3-butanediol aqueous solution was prepared using ultrapure water. 1.0 mL of the Diol aqueous solution was added to 9.0 mL of the citrate modified Au, Ag and Au@Ag NP solution under stirring in the dark for 1 h. After this, the unbound Diol was removed by repeated centrifugation (2500 rpm, 20 min), followed by dispersing the precipitation in 10 mL of pure water to obtain Diol-Ag, Diol-Au and Diol-Au@Ag NP solution.

Synthesis of Raman signal molecular fluorescein phenylboronic acid (Flu-PBA)

3-Aminobenzeneboronic acid (0.175 g, 1.285 mmol) was added to a solution of fluorescein isothiocyanate isomer I (0.50 g, 1.285 mmol) in DMF (5 mL). The reaction mixture was stirred at room temperature for 12 h, and then poured into methanol (10 mL). The solvents were removed *in vacuo*, and the residue was then dissolved in the minimum amount of fresh methanol. Chloroform was added and the product was obtained as a bright orange precipitate (420 mg, 62% yield). ^{1}H NMR

(300 MHz, $CDCl_3$): δH = 7.97 (1H, d, J = 2.7), 7.74 (1H, dd, J = 8.5 and 2.7 Hz), 7.71 (1H, s), 7.6 (1H, d, J = 8.5 Hz), 7.36 (1H, m), 7.19–7.15 (2H, m), 6.63–6.59 (5H, m), 3.35 ppm (2H, NH).

Fabrication of the Raman nanoprobes for F^- detection in water

Briefly, 200 μL of Flu-PBA (5.0 μM) aqueous solution was added into the Diol-modified Au@Ag NP monodispersion (1 mL) in a 1.5 mL centrifuge tube, followed by shaking for 30 min. Then, the unbound Flu-PBA was removed by repeated centrifugation (2500 rpm, 20 min), followed by redispersing the precipitate in 1.0 mL of ultrapure water to obtain the probes Flu-PBA-Diol-Au@Ag NPs. Flu-PBA-Diol-Au and Flu-PBA-Diol-Ag NPs were also fabricated using the same process. The pH of the solution was adjusted to 7.4 by adding 0.1 M NaOH under shaking. Different concentrations of F^- were added into the mixture, respectively. After 10 min reaction, the mixture was first sucked into a capillary glass tube, which was then fixed onto a glass slide. The Raman spectra were recorded using a 532 nm laser with 10 mW power and 10× objective (2.1 μm^2 spot). The integral time was 5 s with 5 rounds of accumulations, and the slit aperture was 50 μm. The experiments were replicated three times for each concentration. Other ions were also detected using the same method.

Preparation of the silica-based SERS chips for F^- detection in real samples

The silica-based SERS chip for the ultrasensitive detection of F^- was fabricated by the assembly of Diol-Au@Ag NPs on a piece of silicon substrate, and further covalently linked with the Raman-signal molecules Flu-PBA. Au@Ag NPs were assembled on a silicon substrate in the following procedure: first, a silicon substrate was cleaned by sequential ultrasonication in acetone, ethanol, and ultrapure water for 15 min in sequence, and then treated with H_2SO_4–H_2O_2 (3 : 1 v/v) at 60 °C for 30 min to derive a hydroxyl surface. After thorough rinsing with ultrapure water and ethanol, the cleaned silicon substrate was dried in air. Second, the cleaned silicon substrate was immersed into 10% APTS ethanol solution for 18 h to silanize the substrate with an $-NH_2$ end group. The substrate was then extensively rinsed with ethanol to remove the unbound monomer from the surface and dried in air. Third, the $-NH_2$ modified silicon wafer was submerged into colloidal Diol-Au@Ag NPs for 12 h, resulting in the formation of a layer of Diol-Au@Ag NPs on the silicon surface. Finally, after being washed with pure water, the silicon substrate with a layer of Diol-Au@Ag NPs was further immersed into 1.0 μM of Flu-PBA solution for 4 h at room temperature to obtain a silica-based SERS chip for the selective detection of F^-.

A volume of 2 mL of F^- solution with different concentrations was spiked into 2 mL of tap water and lake water, followed by adjusting the pH of the solution to 7.4. After centrifugation, the clear supernatant was collected and filtered through 0.45 μm Supor filters to remove any particulate suspension. Prior to the assay, the samples were diluted 100 times with ultrapure water so that the level of F^- was within the linear range. Then, 20 μL of the sample solution was evenly dropped onto the modified SERS chip. The time resolved Raman spectra were immediately recorded with a 532 nm laser with 5 mW power and 50× objectives (1 μm^2 spot). The integral time was 10 s, and the slit aperture was 50 μm. The interval period for the collection of the Raman spectra was set at 20 s.

Characterization and instruments

The prepared Au@Ag NPs were characterized by field-emission scanning microscopy (FE-SEM, Sirion 200) and transmission electron microscopy (TEM, JEOL 2010), respectively. UV-vis absorption spectra were recorded with a Shimadzu UV-2550 spectrometer. High-resolution mass spectra (HR-MS) were obtained using an Agilent Q-TOF 6540 mass spectrometer. Raman measurements were conducted with a Thermo Fisher DXR Raman microscope equipped with a CCD detector. Infrared spectra of the dried Au@Ag NPs, Diol-Au@Ag NPs, and Flu-PBA-Diol-Au@Ag NPs dispersed in KBr pellets were recorded on a Thermo-Fisher Nicolet iS10 FT-IR spectrometer. Photographs were taken with a Canon 350D digital camera.

Results and discussion

Fig. 1 illustrates the SERS sensing mechanism for detection of F^- by employing the Raman probe Flu-PBA-Diol-Au@Ag NPs. The as-synthesized Au@Ag NPs have an average size of ~45 nm, and the thickness of the silver shell is ~7 nm, which was grown by a seeded growth method *via* a consecutive two-step process (see the TEM images of Fig. S1 in the ESI†).[35] Due to the wide and strong plasmon resonance, Au@Ag NPs have been reported to exhibit the highest Raman enhancement effects compared to Au and Ag NPs and used as SERS nanosensors for the detection of pesticide residues at fruit surfaces and in fruit juices.[36] Due to the existence of –SH groups, each 1,4-dimercapto-2,3-butanediol molecule can adsorb intensely onto the silver shells of Au@Ag NPs by the intense Ag–S covalent bond.[37,38] According to previous reports, it is easy to

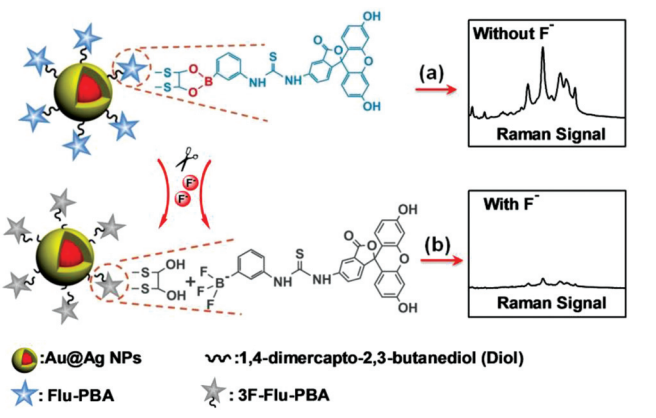

Fig. 1 Schematic illustration of Flu-PBA-Diol-Au@Ag NPs in (a) the absence and (b) the presence of F^-, and the corresponding SERS responses.

form a cyclic boronate ester between boronic acid and diol for their tight but reversible affinity.[39,40] Being a remarkable Raman active resonant dye, fluorescein phenylboronic acid (Flu-PBA) can covalently bond to the surface of Diol-Au@Ag NPs through the formation of a cyclic boronate ester (as drawn in Fig. 1a), leading to a strong surface-enhanced Raman effect and SERS signal readouts. On the other hand, among all anions with a minimal radius, the fluoride anion is a 'hard base' among all anions with a minimal radius, while the center atom of the cyclic boronate ester bond, boron, is a 'hard acid'. Boron possesses an empty p orbit which is willing to accept an external lone pair electron.[41,42] Thus, fluoride ions could strongly interact with the boron atom. After the addition of fluoride ions, the configuration of the center atom boron changed from sp^2 trigonal hybridization to sp^2–sp^3 tetrahedron hybridization, which could disturb the combination between boronic acid and diol.[43,44] Therefore, the Flu-PBA-Diol-Au@Ag NP probes were converted to the corresponding trifluoroborate anion (3F-Flu-PBA) and Diol-Au@Ag NPs, resulting in the exfoliation of Raman active molecules from the surface of Diol-Au@Ag NPs. The strong Raman signals of Flu-PBA cannot be detected at all due to the lack of the surface-enhanced Raman effect. As a result, F^- can quench the strong Raman signals of Flu-PBA-Diol-Au@Ag NPs in the SERS sensor, providing an ultrasensitive detection method.

The above concept for the detection of F^- has been further evidenced by UV-vis, FT-IR, HR-MS, and Raman spectroscopy characterization and TEM examinations. The bright orange Au@Ag NPs had a wide range of plasmon resonance absorption from 320 to 560 nm, resulting from the overlapping and interaction of two different plasmon resonance frequencies of Au cores and Ag nanoshells in the core–shell nanoparticles as shown in Fig. 2A. With the increase of Diol concentration from 1.0×10^{-7} to 7.5×10^{-5} M in the colloid, UV-vis spectroscopy revealed that the absorbance of Au@Ag NPs decreased gradually (see the part A of Fig. S2 in the ESI†). The color of Au@Ag NPs changed from orange to light brown (the inset of Fig. S2-part A†), which indicated the formation of the Diol-Au@Ag NPs and the aggregation of Au@Ag NPs induced by the excessive Diol. This was further confirmed by the TEM observations: the monodisperse Au@Ag NPs in the absence of Diol and the significant aggregation of Au@Ag NPs in the presence of 7.5×10^{-5} M Diol (parts B and C of Fig. S2,† respectively). As shown in Fig. 1, the Diol molecule has two thiolated groups to bind Ag shells and thus play a role of cross-linking agent to effectively induce the occurrence of colloidal aggregation. However, the aggregation makes the next accurate functional modification at the surface of colloidal Au@Ag NPs and the determination of F^- almost impossible. Finally, the concentration of Diol to modify the Au@Ag NPs was selected to be approximately 1.0×10^{-6} M for avoiding the unexpected aggregation. The prepared Diol functional colloid can remain stable in the monodispersive state for at least one week that is long enough for further use in the detection.

Fluorescein has been regarded as a useful standard Raman signal molecule for the evaluation of the SERS performance

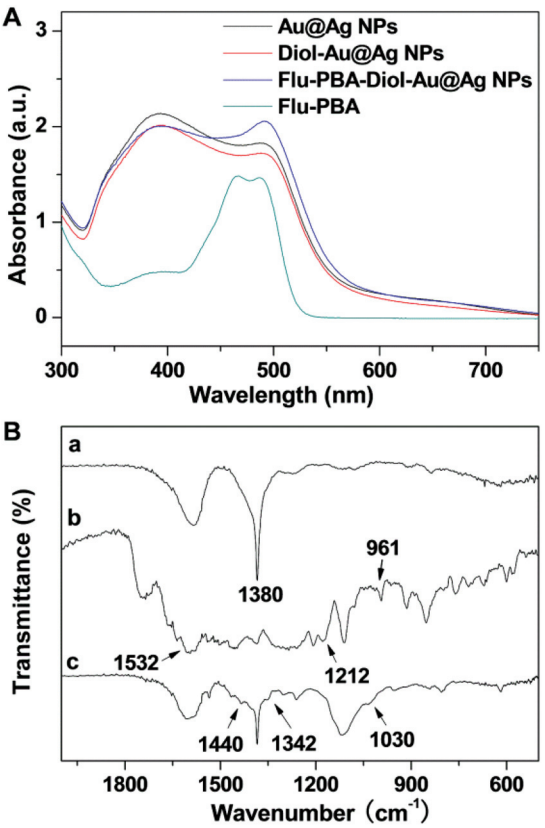

Fig. 2 (A) UV-vis absorption spectra of Au@Ag NPs, Diol-Au@Ag NPs, Flu-PBA-Diol-Au@Ag NP colloids and Flu-PBA aqueous solution, respectively. (B) FTIR spectra of (a) Diol-Au@Ag NPs, (b) pure Flu-PBA (c) the prepared Flu-PBA-Diol-Au@Ag NP probes.

because of its high Raman scattering cross-sections. For the sensing design, a new boronic acid derivative of fluorescein was prepared as shown in the Experimental section. The NCS derivative of fluorescein was stirred in dimethylformamide with 3-aminophenylboronic acid at room temperature for 12 h to furnish the thiourea linked boronic acid fluorescein conjugate Flu-PBA in 62% yield. Upon the addition into the Diol-Au@Ag NP solution, Flu-PBA, which acted as a diol receptor, could covalently reversibly combine with Diol-Au@Ag NPs to form five or six-membered cyclic boronate ester complexes. The color of Flu-PBA-Diol-Au@Ag NPs still remains orange which indicates that the Au@Ag NPs were well dispersed in aqueous solution and the aggregation of Au@Ag NPs would not occur. The formation of Flu-PBA-Diol-Au@Ag NP probes can be confirmed by UV-visible absorption spectra, FT-IR spectra and SERS spectra. The UV-visible absorption peak obviously shifts from 500 to 495 nm, which can be explained in terms of the interactions between Flu-PBA and the plasmons of metallic nanoparticles (see Fig. 2A). The FT-IR spectrum of the Flu-PBA-Diol-Au@Ag NPs exhibits distinct absorption bands at 1440, 1342 and 1030 cm^{-1}, which can be attributed to the C–B stretching vibration, B–O–C bending vibration and B–O–C deformation vibration, respectively.[45] Meanwhile, the characteristic IR absorption peaks at 1212 and 961 cm^{-1}

disappear due to the B–O–H bending vibration and B–O–H deformation vibration (see Fig. 2B).[46] These results indicate that the Raman signal molecules Flu-PBA are successfully bonded to the Diol-Au@Ag NP surface by the cyclic boronate esters formation. As a result, the Raman signals of Flu-PBA became significantly stronger, the typical Raman peaks of Flu-PBA including 1173, 1308, 1487, 1538, and 1625 cm^{-1} can be clearly detected (as illustrated in Fig. S3-part A and the assignments of peaks in Fig. S3-part B in the ESI†), which implies the formation of hot spots at the surface of Flu-PBA-Diol-Au@Ag NPs (as illustrated in Fig. 3A). Although similar behaviors also occurred in the pure Ag and Au NP colloid, the enhancement effect of Au@Ag NPs was ~6.28- and 4.0-fold those of pure Au and Ag NPs, respectively (see Fig. S4 in the ESI†). The better enhanced effect may result from the coupling of the plasmon resonance of Ag nanoshells and Au cores.

It is interesting that the addition of F^- can obviously inhibit the occurrence of the surface-enhanced Raman effect and quench the Raman intensity of the resulting nanoprobes. Under optical conditions (Fig. S5 and S6 in the ESI†), the effect of the F^- concentration on the SERS intensity was investigated under the constant concentration of Flu-PBA at 1.0×10^{-6} M. The Raman signals of Flu-PBA in this system gradually decreased with the increase of F^- concentration from 1.0×10^{-9} to 1.0×10^{-6} M (Fig. 3A). Even at the concentration of 1.0×10^{-9} M, the intensity of the strongest peak at 1308 cm^{-1} decreased by about 6.8%, revealing the high sensitivity of this SERS system to F^-. When the concentration of F^- increased to 1.0×10^{-6} M, the Raman signal was almost decreased to that of bare Diol-Au@Ag NPs. These confirm that the extremely strong fluoride–boron interaction leads to the cleavage of the Flu-PBA-Diol-Au@Ag NP complex and the surface-enhanced Raman effect will not occur. The reactions of F^- with Flu-PBA-Diol-Au@Ag NPs and the resultant complex structures were further confirmed by HR-MS spectra. Fig. 3B shows the HR-MS spectra of the mixtures of F^- with the Flu-PBA-Diol-Au@Ag NPs in aqueous solution. After the F^- was mixed with nanoprobes in solution, the sodiation of the 3F-Flu-PBA complex peak at m/z = 572.09 was clearly detected (Fig. 3B), suggesting the occurrence of the cleavage reaction of cyclic boronate esters and the formation of the trifluoroborate anion complex in the system. The disappearance of the characteristic FT-IR absorption peak of the boronate ester bond (1440, 1342 and 1030 cm^{-1}) further evidenced that F^- caused the breakage of the cyclic boronic ester bond from another aspect (see Fig. S7 in the ESI†). Accordingly, in the presence of F^-, the Flu-PBA-Diol-Au@Ag NP probes were rapidly broken by strongly binding B–F to form a more stable complex because the B–F bond has a stronger coordinative ability than the B–O bond.

Meanwhile, the specificity of this system to F^- was tested by the SERS response upon the addition of other anions (1.0×10^{-5} M) without and with the coexistence of F^- (1.0×10^{-6} M) in the probe solution. Ions such as Cl^-, Br^-, I^-, HCO_3^-, CO_3^{2-}, HPO_4^{2-}, NO_3^- and SO_4^{2-} did not exhibit the quenching effect to SERS signals of Flu-PBA-Diol-Au@Ag NP probes (as shown in Fig. 4C). Only F^- gave a significant quenching Raman effect in the

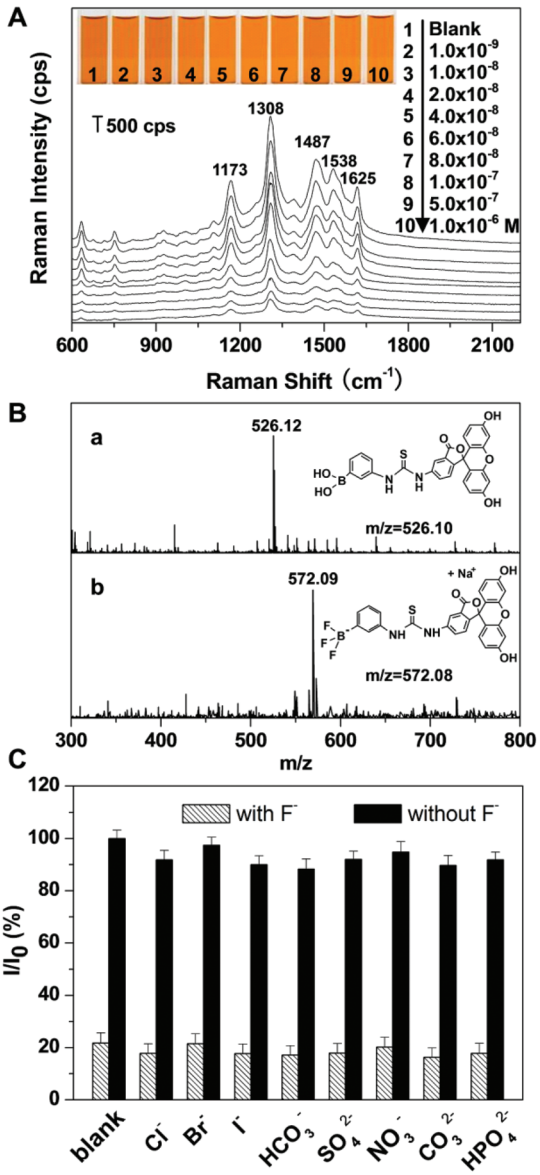

Fig. 3 (A) SERS spectra of Flu-PBA-Diol-Au@Ag NP probes with the increase of F^- concentration from 1.0×10^{-9} to 1.0×10^{-6} M (the inset is the corresponding color images). (B) HR-MS spectra of (a) pure Flu-PBA, and (b) the products of 3F-Flu-PBA after the mixtures of F^- with Flu-PBA-Diol-Au@Ag NP colloids, respectively. (C) Selectivity of the Flu-PBA-Diol-Au@Ag NP probes in addition to the other anions (1.0×10^{-5} M) without and with the coexistence of F^- (1.0×10^{-6} M). The SERS intensity of the peak at 1308 cm^{-1} was used for the evaluation of the Raman signals.

aqueous solution. These above observations reveal the high selectivity of this SERS system to F^- by the use of Flu-PBA-Diol-Au@Ag NP probes. Through experiment, we also found that the HS^- could also quench the SERS signal of the probe to a certain extent (see Fig. S8 in the ESI†). However, the interference of HS^- in the detection of F^- could be effectively avoided by the addition of *N*-ethylmaleimide (NEM) as a chelating agent. The high selectivity of the present probes towards F^- over other anions can be attributed to the highest Lewis basicity of the fluoride ions

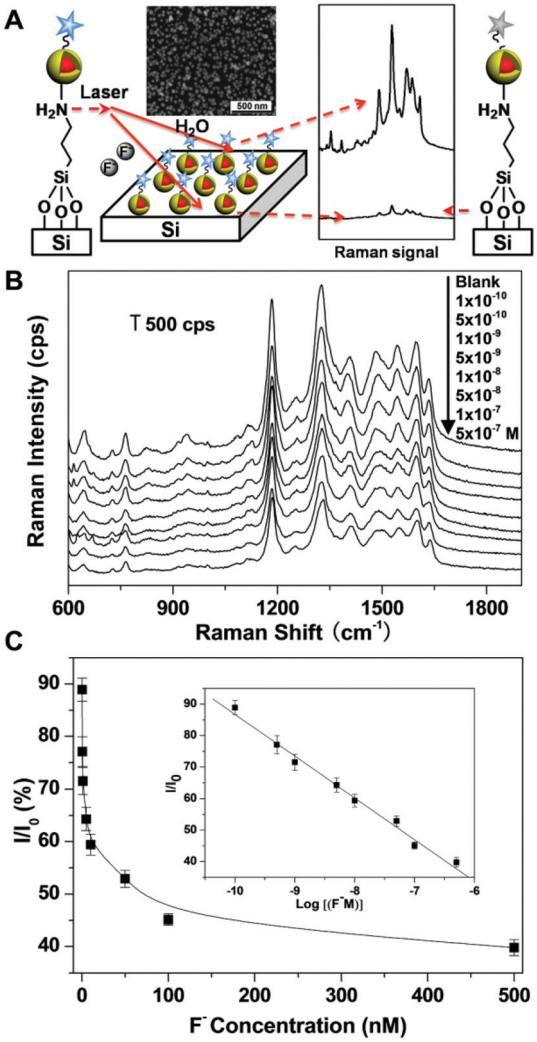

Fig. 4 (A) Schematic drawing for the detection of F^- with the SERS chip fabricated by the assembly of Diol-Au@Ag NPs on a silicon wafer, and further modified with Flu-PBA molecules. (B) Evolution of SERS spectra of Flu-PBA with the addition of an aqueous F^- droplet. (C) Plot of SERS quenching as a function of the F^- concentrations. The inset is the linear correlation of Raman intensity (at 1308 cm^{-1}) with the logarithm of F^- concentrations from 1.0×10^{-10} to 5.0×10^{-7} M. I_0 and I are the peak of SERS at 1308 cm^{-1} of the SERS chip in the absence and in the presence of F^-, respectively.

among all anions and the minimal radius of fluoride ions, further promoting the strong binding of F^- to the boron atom.

On the basis of the above concept, a silica-based SERS chip for the ultrasensitive detection of F^- has been fabricated by the assembly of Diol-Au@Ag NPs on a piece of silicon wafer, followed by modification with Flu-PBA molecules at a concentration of 1.0×10^{-6} M (see the details in the Experimental section). 3-Aminopropyltriethoxysilane (3-APTS) was first linked onto the surface of the chemically treated silicon wafer to form a monolayer of APTS with the $-NH_2$ end group, as shown in Fig. 4A. When the wafer was immersed into the Diol-Au@Ag NP colloid, the Diol-Au@Ag NPs automatically adsorbed onto the surface of the wafer by the interaction between the particles and the $-NH_2$ end groups, resulting in a dense/stable monolayer of Diol-Au@Ag NPs on the substrate. Subsequently, the SERS chip was further bonded with Flu-PBA in solution to obtain strong and uniform Raman readouts of Flu-PBA (Fig. S9 in the ESI†). Importantly, when a droplet of 20 μL of pure water was added onto this chip, the Raman intensity focused on the droplet was unchangeable (Fig. S10 in the ESI†), indicating the stable adsorption of Flu-PBA at the monolayer of Au@Ag NPs. In contrast, the Raman signals of Flu-PBA obviously quenched if the same water droplet containing F^- was added onto the chip, which is attributed to the exfoliation of Flu-PBA molecules from the monolayer of Au@Ag NPs into the liquid droplet (Fig. S10 in the ESI†). The quenching degree reached the maximum and was kept stable after ~10 min. Meanwhile, the silica-based SERS chip could be kept stable for 3 weeks in the vacuum drying environment (Fig. S11 in the ESI†). Therefore, the SERS chip can be used for the fast detection of trace F^- with a very little amount of sample.

Fig. 4B shows the Raman test results by adding a droplet of 20 μL of water containing different concentrations of F^-. With the increase in the concentration of F^- from 1.0×10^{-10} to 5.0×10^{-7} M, the Raman intensity of the resulting nanoprobes dramatically decreased. With the increase in the concentration of F^- from 1.0×10^{-10} to 5.0×10^{-7} M, the Raman intensity of the resulting silica-base SERS chip dramatically decreased (as shown in Fig. 4). Meanwhile, the SERS intensity varied more sensitively with F^- at low concentrations (typically <5 nM). In contrast, the SERS intensity decreased slower and seemed to reach a plateau at a higher F^- concentration. It has been reported that enough of nanoprobes could increase the cleavage reaction rate of the cyclic boronate ester in the presence of F^-.[47] Therefore, it is speculated that the addition of a higher level of F^- could induce more consumption of Flu-PBA-Diol-Au@Ag NP probes, which was not beneficial for the subsequent detection of F^- (due to the lack of nanoprobes) and could hardly have the same rate in the subsequent reaction of residual nanoprobes. Fortunately, a plot of I/I_0 (the ratio of SERS intensity at 1308 cm^{-1} in the presence and absence of F^-) *versus* F^- concentrations shows a linear correlation in the concentration range from 0.1–500 nM. The calibration equation was $I/I_0 = -45.7285-13.2474\lg C_{F^-}$ (where $R^2 = 0.993$, C_{F^-} is the concentration of F^-). Statistical analysis reveals a limit of detection of F^- as low as 0.1 nM, which was calculated based on three standard deviations above the background. The high sensitivity of SERS chips towards F^- indicated the strong binding of F^- to the boron atom, leading to the breaking of the cyclic boronate ester to form a more stable complex trifluoroborate anion (3F-Flu-PBA). The 3F-Flu-PBA exfoliated from the chip into the aqueous F^- droplet resulted in the quenching of Raman signals of Flu-PBA. The excellent specificity of the SERS chip to F^- was also demonstrated as shown in Fig. S12.†

In order to verify the usefulness of the proposed sensor for the identification and detection of F^- in practical applications, the detection of natural F^- in real samples (tap water and lake water) was demonstrated here by the use of the SERS silica-chip (Fig. S13 in the ESI†). The results have been compared

Table 1 Real determination and recovery test of F^- in different samples

Sample	IC method[a] (μmol L^{-1})	Proposed SERS method[b] (nmol L^{-1})	Spiked F^- (nmol L^{-1})	Measured F^- (nmol L^{-1})	Recovery (%)	RSD (%)
Tap water	14.59	7.27	100.0	96.10	88.79	3.28
			200.0	186.90	89.81	7.62
			500.0	471.50	92.85	5.95
Lake water	17.80	8.93	100.0	97.20	88.29	3.44
			200.0	208.90	99.98	4.59
			500.0	538.00	105.80	6.17

[a] The data represent natural F^- levels detected by ion chromatography (IC). [b] The F^- concentrations were obtained after a total of 200 times dilution with ultrapure water.

with those obtained by ion chromatography (IC) and are listed in Table 1, standard recovery experiments were also carried out. The samples only need to be pretreated with simple incubation and centrifugation (see the Experimental section). Prior to the assay, the samples were diluted 100 times with ultrapure water so that the level of F^- was within the linear range. The data listed in Table 1 indicated that the obtained results were highly consistent with those from the ion chromatography (IC) method, and the recovery of F^- ranged from 88.29% to 105.80%. All the experimental results confirmed that the SERS chip had a high accuracy, reliability, and sensitivity to meet the requirements in practical applications.

Conclusions

In summary, we have presented a novel SERS nanosensor for the rapid, selective, and sensitive detection of fluoride ions. By covalently linking with fluorescein phenylboronic acid to the surface of Diol-Au@Ag NPs, both F^- responsiveness and SERS activity are integrated into the Flu-PBA-Diol-Au@Ag NP nanosensor. In the presence of fluoride ions, the specific cyclic boronate esters between Flu-PBA and the diol of the nanosensors are converted to trifluoroborate anions and Diol-Au@Ag NPs, which causes the exfoliation of 3F-Flu-PBA from the surface of Diol-Au@Ag NP, resulting in the quenching of SERS signals. Furthermore, we have successfully fabricated a silica-based SERS chip by assembling the nanosensor (core–shell Flu-PBA-Diol-Au@Ag NPs), and the SERS chip achieved an ultrahigh sensitivity to F^- at the nanomolar level. Our developed silica-based SERS chips possess many advantages, such as excellent anti-interference ability, portable feasibility, and simple operation. On the other hand, the detection method only needs a very little amount of sample, and is very simple and inexpensive compared to earlier methods. This SERS-chip technique may be extended to open a novel avenue to develop various SERS-based sensors for Raman-inactive molecules.

Acknowledgements

This work is supported by the National Basic Research Program of China (2015CB932002), the China-Singapore Joint Project (2015DFG92510), the Science and National Natural Science Foundation of China (no. 21507134, 21371174, 21671052), the Natural Science Foundation of Anhui Province (1408085QB29, 1508085QB29), the Scientific Research Foundation of Anhui Agricultural University (Grant No. yj2016-06), and the Youth Research Foundation of Anhui Agricultural University (2015zr007).

References

1 P. A. Gale, *Coord. Chem. Rev.*, 2001, **213**, 79–128.
2 P. D. Beer and P. A. Gale, *Angew. Chem., Int. Ed.*, 2001, **40**, 486–516.
3 Y. Zhou, J. F. Zhang and J. Y. Yoon, *Chem. Rev.*, 2014, **114**, 5511–5571.
4 H. S. Horowitz, *J. Public Health Dent.*, 2003, **63**, 3–8.
5 J. R. Farley, J. E. Wergedal and D. J. Baylink, *Science*, 1983, **222**, 330–332.
6 M. Kleerekoper, *Endocrinol. Metab. Clin. North Am.*, 1998, **27**, 441–452.
7 M. L. Cittanova, B. Lelongt and M. C. Verpont, *Anesthesiology*, 1996, **84**, 428–435.
8 P. P. Singh, M. K. Barjatiya, S. Dhing, R. Bhatnagar, S. Kothari and V. Dhar, *Urol. Res.*, 2001, **29**, 238–244.
9 http://water.epa.gov/drink/contaminants/index.cfm.
10 J. Fawell, K. Bailey, J. Chilton, E. Dahi, L. Fewtrell and Y. Magara, *Fluoride in Drinking-water*, World Health Organization (WHO), IWA Publishing, 2006.
11 Y. P. Hang and C. Y. Wu, *Anal. Chim. Acta*, 2010, **661**, 161–166.
12 D. A. P. Tanaka, S. Kerketta, M. A. L. Tanco, T. Yokoyama and T. M. Suzuki, *Sep. Sci. Technol.*, 2002, **37**, 877–894.
13 R. A. Rocha, D. Rojas, M. J. Clemente, A. Ruiz, V. Devesa and D. Velez, *J. Agric. Food Chem.*, 2013, **61**, 10708–10713.
14 I. C. Guimarães, C. C. Rezende, J. A. F. Silva and D. P. Jesus, *Talanta*, 2009, **78**, 1436–1439.
15 X. M. Qian and S. M. Nie, *Chem. Soc. Rev.*, 2008, **37**, 912–920.
16 L. G. Xu, H. H. Yin, W. Ma, H. Kuang, L. B. Wang and C. L. Xu, *Biosens. Bioelectron.*, 2015, **67**, 472–476.
17 S. Li, L. G. Xu, W. Ma, H. Kuang, L. B. Wang and C. L. Xu, *Small*, 2015, **11**, 3435–3439.

18 S. Schlücker, *Angew. Chem., Int. Ed.*, 2014, **53**, 4756–4795.
19 L. J. Tang, S. Li, F. Han, L. Q. Liu, L. G. Xu, W. Ma, H. Kuang, A. K. Li, L. B. Wang and C. L. Xu, *Biosens. Bioelectron.*, 2015, **71**, 7–12.
20 L. G. Xu, H. H. Yin, W. Ma, H. Kuang, L. B. Wang and C. L. Xu, *Biosens. Bioelectron.*, 2015, **67**, 472–476.
21 H. X. Xu, J. Aizpurua, M. Kall and P. Apell, *Phys. Rev. E: Stat. Phys., Plasmas, Fluids, Relat. Interdiscip. Top.*, 2000, **62**, 4318–4324.
22 A. Campion, J. E. Ivanecky, C. M. Child and M. Foster, *J. Am. Chem. Soc.*, 1995, **117**, 11807–11808.
23 K. Kneipp, H. Kneipp and J. Kneipp, *Acc. Chem. Res.*, 2006, **39**, 443–450.
24 S. S. R. Dasary, A. K. Singh, D. Senapati, H. Yu and T. P. C. Ray, *J. Am. Chem. Soc.*, 2009, **131**, 13806–13812.
25 L. Y. Bi, Y. Y. Rao, Q. Tao, J. Dong, T. Su, F. J. Liu and W. P. Qian, *Biosens. Bioelectron.*, 2013, **43**, 193–199.
26 W. H. Lin, Y. H. Lu and Y. J. Hsu, *J. Colloid Interface Sci.*, 2014, **418**, 87–94.
27 L. Qiu, W. Q. Wang, A. W. Zhang, N. N. Zhang, T. Lemma, H. H. Ge, J. J. Toppari, V. P. Hytonen and J. Wang, *ACS Appl. Mater. Interfaces*, 2016, **8**, 24394–24403.
28 R. A. Alvarez-Puebla and L. M. Liz-Marzan, *Angew. Chem., Int. Ed.*, 2012, **51**, 11214–11223.
29 V. Amendola and M. Meneghetti, *Adv. Funct. Mater.*, 2012, **22**, 353–360.
30 L. Y. Zhang, Y. Jin, X. Y. Huang, Y. J. Zhou, S. H. Du and Z. P. Zhang, *Anal. Chem.*, 2015, **87**, 11763–11770.
31 J. Wang, L. Yang, B. Liu, H. Jiang, R. Liu, J. Yang, G. Han, Q. Mei and Z. Zhang, *Anal. Chem.*, 2014, **86**, 3338–3345.
32 D. W. Li, L. L. Qu, K. Hu, Y. T. Long and H. Tian, *Angew. Chem., Int. Ed.*, 2015, **54**, 12758–12761.
33 Y. X. Du, R. Y. Liu, B. H. Liu, S. H. Wang, M. Y. Han and Z. P. Zhang, *Anal. Chem.*, 2013, **85**, 3160–3165.
34 D. Grasseschi, V. M. Zamarion, K. Araki and H. E. Toma, *Anal. Chem.*, 2010, **82**, 9146–9149.
35 B. H. Liu, G. M. Han, Z. P. Zhang, R. Y. Liu, C. L. Jiang, S. H. Wang and M. Y. Han, *Anal. Chem.*, 2012, **84**, 255–261.
36 M. Rycenga, C. M. Cobley, J. Zeng, W. Y. Li, C. H. Moran, Q. Zhang, Q. Dong and Y. N. Xia, *Chem. Rev.*, 2011, **111**, 3669–3712.
37 M. Xue, X. Wang, L. L. Duan, W. Gao, L. F. Ji and B. Tang, *Biosens. Bioelectron.*, 2013, **39**, 82–87.
38 X. C. Chen, S. M. Yu, L. Yang, J. P. Wang and C. L. Jiang, *Nanoscale*, 2016, **8**, 13669–13677.
39 Y. S. Xia and P. F. Shen, *Anal. Chem.*, 2014, **86**, 5323–5329.
40 A. P. Liu, S. Peng, J. C. Soo, M. Kuang, P. Chen and H. W. Duan, *Anal. Chem.*, 2011, **83**, 1124–1130.
41 C. R. Cooper, N. Spencer and T. D. James, *Chem. Commun.*, 1998, **13**, 1365–1366.
42 P. Wu and X. Yan, *Biosens. Bioelectron.*, 2010, **26**, 485–490.
43 Z. P. Liu, L. L. Liu, M. H. Sun and X. G. Su, *Biosens. Bioelectron.*, 2015, **65**, 145–151.
44 Z. Lin, S. C. Qu, D. B. Zhang and Z. Bai, *Chem. Commun.*, 2006, **6**, 624–626.
45 J. A. Faniran and H. F. Shurve, *Can. J. Chem.*, 1968, **46**, 2089–2094.
46 S. H. Brewer, A. M. Allen, S. E. Lappi, T. L. Chasse, K. A. Briggman, C. B. Gorman and S. Franzen, *Langmuir*, 2004, **20**, 5512–5520.
47 Y. Y. Bao, B. Liu, F. F. Du, J. Tian, H. Wang and R. K. Bai, *J. Mater. Chem.*, 2012, **22**, 5291.